Modeling the Critical Current of Polycrystalline Superconducting Films in High Magnetic Fields

Alexander I. Blair and Damian P. Hampshire

***Abstract*—We have performed simulations using time-dependent Ginzburg–Landau theory on a two-dimensional (2-D) polycrystalline system, where grain boundaries are modeled as narrow regions with a locally reduced critical temperature (T_c). For the small system sizes investigated, we find that the critical current density (J_c) is not sensitive to changes in grain size until the grain size is sufficiently small that it limits the average superparticle density in the system through the proximity effect. Furthermore, once T_c in the boundary regions is sufficiently low relative to the surrounding superconductor that grain boundary regions act as preferred channels for flux flow, further reductions in the boundary T_c only weakly reduce J_c across the superconductor.**

***Index Terms*—TDGL, thin films, junctions, critical current density.**

I. Introduction

THERE is considerable interest in predicting and modelling the critical current density (J_c) characteristics in high magnetic fields of superconductors with different microstructures for applications such as fusion magnets. Grain boundary structures are of particular interest because most technological superconductors used in large scale applications are polycrystalline and these structures strongly affect flux distribution in superconductors and limit J_c [1]. Modelling grain boundaries as junction systems, [2] has led to simulations of J_c as a function of field for a superconductor containing a periodic series of 'weak links' of reduced T_c. First attempts to model the critical current density of a large-scale 3D polycrystalline systems have also been carried out [3], but have so far been restricted to periodic grain morphologies. Sadovskyy et al. [4] have modelled J_c from the experimentally determined pinning landscape in a quasi-single-crystalline YBCO sample, using a scalable time-dependent Ginzburg—Landau (TDGL) solver in the high-κ limit for fast computation on GPU architectures [5], and developed it to predict microstructures that optimize J_c [6], [7].

In this paper we use Voronoi tessellations to generate the grain morphology, which have become state-of-the-art for modelling mesoscale polycrystalline systems [8]. The D-dimensional Voronoi tessellation of a region containing a set of n seed points is a collection of n D-dimensional polyhedra (grains) whose interior consists of all points that are closer to a given seed point than any other. Physically, this corresponds to a polycrystalline material in which all grains nucleated at the same time and grew isotropically at identical rates [9]. This approach generates structures that qualitatively agree with real polycrystal grain sizes and nearest neighbor distributions to first order [9] and have been used in a wide range of polycrystal simulations, including those considering the effect of grain size on grain boundary resistivity [10]. We investigate the effect of reducing the local T_c in grain boundary regions of a two-dimensional Voronoi polycrystal on the field-dependence of J_c using simulations based on TDGL theory. We also compare this to a similar simple system with a single Josephson junction.

Manuscript received October 30, 2018; accepted January 9, 2019. Date of publication January 24, 2019; date of current version February 19, 2019. This work was supported in part by EPSRC under Grant EP/L01663X/1 that supports the EPSRC Centre for Doctoral Training in the Science and Technology of Fusion Energy, and has been carried out within the framework of the EUROfusion Consortium, and in part by the Euratom research and training programme 2014–2018 under Grant 633053. *(Corresponding author: Alexander I. Blair.)*

The authors are with the Durham University, Department of Physics, Superconductivity Group, South Road, Durham, DH1 3LE, U.K. (e-mail: a.i.blair@durham.ac.uk).

Color versions of one or more of the figures in this paper are available online at http://ieeexplore.ieee.org.

Digital Object Identifier 10.1109/TASC.2019.2895213

II. Theory and System Geometry

The TDGL equations have been derived by Gor'kov and Eliashberg [11] for gapless superconductors dominated by paramagnetic impurities at temperatures close to their critical temperature. They can be written in normalized form [5], [12] for an isotropic material with uniform effective mass m and resistivity ρ. In the simulations presented here, all parameters are normalized relative to GL material parameters of the principal superconductor α_s, β_s, m_s and ρ_s. Distances are normalized in units of the superconductor coherence length $\xi_s = \hbar/\sqrt{2m_s\alpha_s}$ and time in units of $\tau = \mu_0\kappa^2\xi_s^2/m_s$ where the Ginzburg—Landau parameter $\kappa^2 = 2m_s^2\beta_s/e_s^2\hbar^2\mu_0$. The order parameter is normalized in units of the bulk Meissner state order parameter $|\psi_s| = \sqrt{-\alpha_s/\beta_s}$ and the magnetic vector potential in units of $A_s = \phi_0/2\pi\xi_s = B_{c2}\xi_s$, where ϕ_0 is the magnetic flux quantum and B_{c2} is the upper critical field of the superconductor. Current densities are normalized by the depairing current of the bulk superconductor $J_D = 2B_{c2}/3\sqrt{3}\mu_0\xi_s\kappa^2$ and the electric fields normalized by E_D where $E_D = \rho_s J_D$. In the zero electric potential gauge, the normalized GL equations are given by:

$$\eta\partial_t\psi = \left[(\boldsymbol{\nabla} - \imath\boldsymbol{A})^2 + \epsilon(\boldsymbol{r}) - \beta|\psi|^2\right]\psi, \tag{1}$$

$$\partial_t\boldsymbol{A} = -\kappa^2\left(\boldsymbol{\nabla}\times\boldsymbol{\nabla}\times\boldsymbol{A}\right) + \mathrm{Im}\left[\psi^*\left(\boldsymbol{\nabla} - \imath\boldsymbol{A}\right)\psi\right], \tag{2}$$

with associated boundary conditions

$$(\boldsymbol{\nabla}\times\boldsymbol{A} - \boldsymbol{B})\times\hat{\boldsymbol{n}} = \boldsymbol{0}, \tag{3}$$

$$(\boldsymbol{\nabla} - \imath\boldsymbol{A})\,\psi\cdot\hat{\boldsymbol{n}} = -\gamma\psi, \tag{4}$$

where $\hat{\boldsymbol{n}}$ is the outward pointing normal vector at the surface of the boundary of the system. The Ginzburg—Landau parameter κ represents the ratio of the characteristic length scales for variations of the electromagnetic field and variations in the order

parameter, and the friction parameter η represents the ratio in characteristic time scales for evolution of the electromagnetic field and the order parameter field, related to the diffusivity D via $\eta = m_s/\mu_0 D\kappa^2$. The parameters η, β and m are taken to be constant and real throughout the entire system. We note that although complex values for η are needed to investigate the superconducting Hall effect within the framework of TDGL theory [13], we have minimized the number of free parameters of our system by taking the (real) value of $\eta = 5.78$ obtained by Schmid for superconductors in the dirty limit [14]. Taking β to be constant throughout the system does not significantly restrict the solution space when $-\epsilon \gg \beta/\beta_s$, since in non-superconducting regions, the nonlinear term in Eq. (1) is small and β does not strongly affect the spatial distribution of ψ. We have assumed in normalized units $m = \rho = \text{constant}$ everywhere.

Taking the effective mass m to be constant is a severe restriction, as it requires the entire system to have the same normal state resistivity. To minimize the effect of this, a strongly normal coating region with $\epsilon = -10.0$ and a thickness 6.0ξ between the edges of the superconducting system and the (insulating) boundaries of the computational domain, to allow the spatial distribution of normal currents to equilibrate some distance outside the superconducting system of interest.

In this paper we consider spatially-dependent T_c variations in the system. Hence $\epsilon(\boldsymbol{r})$ is the only spatially varying material parameter, defined in terms of the system temperature T, the local critical temperature $T_c(\boldsymbol{r})$ and the critical temperature of the reference superconductor by $\epsilon(\boldsymbol{r}) = \alpha(\boldsymbol{r})/\alpha_s = (T - T_c(\boldsymbol{r}))/(T - T_{cs})$. In the bulk superconductor, the grain boundaries and the coating regions, we take ϵ to be 1.0, ϵ_{GB} (or ϵ_{Junc} for junction systems) and -10.0 respectively. We consider a system periodic in the *x*-direction along the direction of current flow as shown in Fig. 1. At the system boundaries in the *y* direction, the external magnetic field was constrained using $B(y = \frac{w}{2} \pm \frac{w}{2}) = B_{app} \pm \frac{w_s}{2}\mu_0 J_{app}$ where w is the width of the computational domain, w_s is the width of the superconducting region, J_{app} is the applied current and B_{app} is the applied external magnetic field. Furthermore, the surface parameter γ (reciprocal of de Gennes extrapolation length [15]) was specified at the edges of the computational domain to be insulating (i.e., $\gamma = 0$) throughout this work.

III. Computational Method

We have used a finite-difference spatial discretization scheme [16], which follows a link variable method [17] for imposing gauge invariance on the system. The simulation space was discretized into a regular grid of nodes at points $\boldsymbol{r}_{i,j}$ that are separated by a step size h_x and h_y in the *x* and *y* directions. The order parameter ψ and temperature term ϵ were calculated on each node and 'link variables' a^x, a^y parameterizing the discretized magnetic vector potential [17] were defined on links between nodes. This approach means insures that the discretized equations remain gauge invariant [16] but they are highly coupled and nonlinear, and the timescale for evolution of a^x, a^y is much shorter than ψ since $\kappa^2 \gg \eta^{-1}$. Consequently, a block Gauss-Seidel approach is used on the fully coupled system [18]. ψ is first calculated assuming all other variables unchanged from previous timestep. Then a^x, a^y is calculated using the new ψ. Then ψ is updated again, and solution steps continue until convergence of a^x, a^y, ψ to an absolute tolerance of 10^{-7}. For evolving the time variable, a Crank-Nicolson method [16] was used on the linear terms [18]. The equation for ψ was first simplified using the operator splitting method of fractional steps to reduce the operator into product of tridiagonal (cyclic tridiagonal) matrices containing differences in the *y* (*x*) directions. Cyclic tridiagonal systems are solved using a Sherman-Morrison algorithm with the tridiagonal solver provided by the LAPACK package [19]. The equations for a^x, a^y are solved in one solution step using the Intel MKL PARDISO direct parallel sparse solver [20]. This was found to converge faster than solving for a^x and a^y separately using the method of fractional steps with an explicit treatment of cross-coupling terms [16]. Factorization and analysis of the operator needed only to be performed once as the values are time-independent.

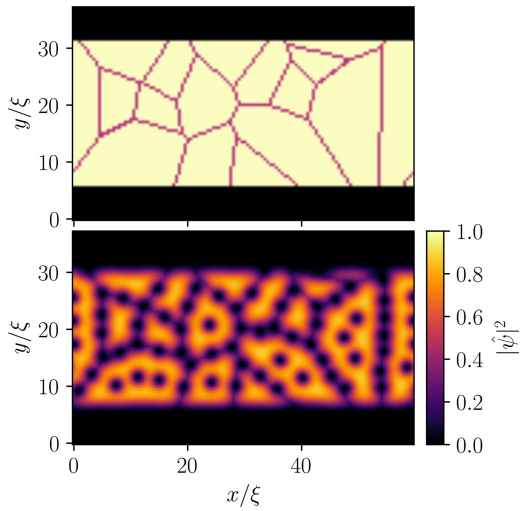

Fig. 1. (Top) Voronoi mesh with 16 grains (top) and a grid step $h_x = h_y = 0.5\xi$ of a superconducting film with $w_s = 25\xi$, $l = 60\xi$, $\eta = 5.79$ and $\kappa = 5$. The effective mass is constant throughout the system. Regions of reduced T_c where $\epsilon = \epsilon_{GB}$ are denoted in red, and coating regions where $\epsilon = -10.0$ are colored black. The edges of each Voronoi cell are 0.5ξ thick. (Bottom) Normalized superparticle density $|\psi|^2$ for this mesh at the critical current density J_c with $\epsilon_{GB} = -1.0$ in an applied magnetic field $B_{app} = 0.35B_{c2}$. The system is periodic in the *x*-direction and insulating boundary conditions were applied at the edges of the computational domain in the *y*-direction.

To generate polycrystalline systems, an unweighted, randomly selected set of *n* nodes within the superconductor region was chosen to be used as seed points for the Voronoi tessellation. The corresponding 2D Voronoi tessellation itself, comprising *n* grains, was generated using the pyvoro Python wrapper [21] to the Voro++ software library [22]. Nodes on the mesh within a distance $d/2$ to the edges of the polygons comprising the Voronoi tessellation were then taken to be grain boundary regions and modelled with $\epsilon = \epsilon_{GB}$. An example is provided in Fig. 1. For comparison, an equivalent Josephson junction system was also modelled, with a single grain boundary region perpendicular to the direction of current flow with the same boundary thickness d used in the polycrystalline simulations.

IV. Results

Fig. 1 shows a representative polycrystalline structure investigated and the corresponding order parameter distribution at J_c. Both inter and intragrain fluxons are present, with a clear preference for fluxons to enter the structure along the grain

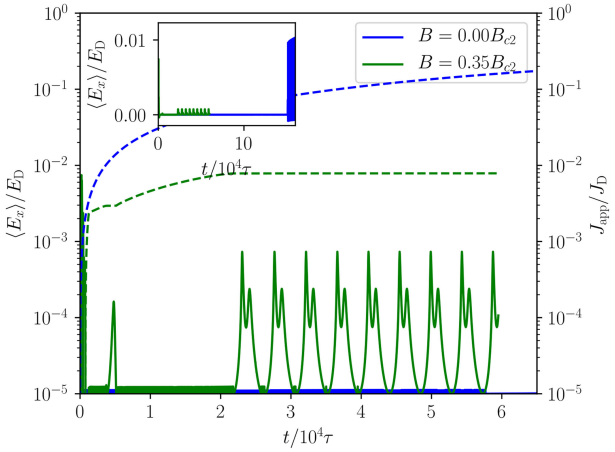

Fig. 2. Average (normalized) electric field in the x-direction $\langle E_x \rangle$ and applied current density $J_{\rm app}$ as a function of simulation time t, denoted by the solid and dashed lines respectively. $J_{\rm app}$ is increased at a rate of $5 \times 10^{-6} J_{\rm D} \tau^{-1}$. The system was initialised in the Meissner state throughout and evolved in timesteps of $h_t = 0.5\tau$. The order parameter and magnetic vector potential were converged to one part in 10^7 at each timestep. The critical current density $J_{\rm c}$ valued stored was taken to be the lowest current at which $E_x > 10^{-5} E_D$ for longer than $2 \times 10^4 \tau$; i.e., persistent vortex motion was observed. Simulations at high magnetic fields take longer to equilibrate, as seen in the figure.

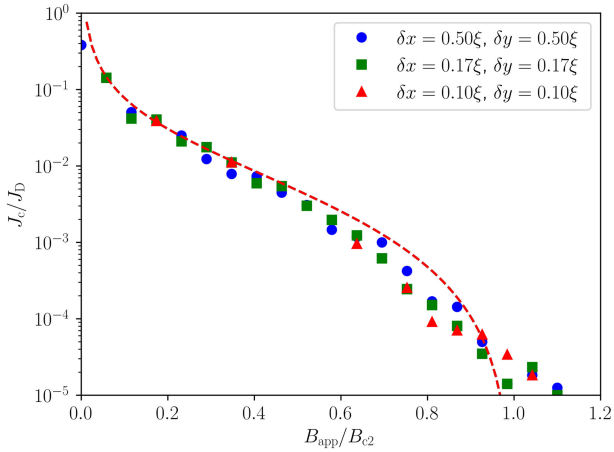

Fig. 3. Critical current density $J_{\rm c}$ as a function of applied magnetic field $B_{\rm app}$ for the Voronoi polycrystalline system shown in Fig. 1 for different mesh sizes. We have used $w_{\rm s} = 25\xi, l = 60\xi, \eta = 5.79$ and $\kappa = 5$. The width of the boundary region in which $T_{\rm c}$ is reduced is unchanged. Mesh size does strongly affect the form of $J_{\rm c}(B)$ obtained. Dashed line represents predicted $J_{\rm c}(B)$ from Eq. 6 with $\epsilon_{\rm Junc} = \epsilon_{\rm GB} = -1$

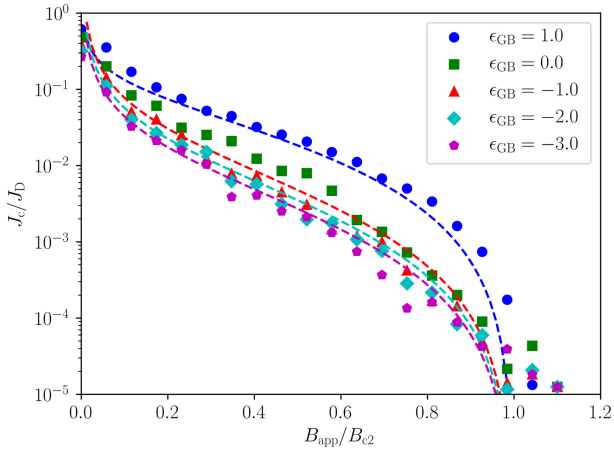

Fig. 4. Critical current density $J_{\rm c}$ as a function of applied magnetic field $B_{\rm app}$ for the Voronoi polycrystalline system shown in Fig. 1 for different $T_{\rm c}$ (i.e., $\epsilon_{\rm GB}$) values in the junction regions. We have used $h_x = h_y = 0.5\xi$, $w_{\rm s} = 25\xi, l = 60\xi, \eta = 5.79$ and $\kappa = 5$. When the junction region is strongly normal, finite-size effects associated with flux quantisation, become important and cusps become visible in the $J_{\rm c}(B)$ characteristic. Dashed lines represented predicted $J_{\rm c}(B)$ from Eq. 5 for $\epsilon_{\rm Junc} = \epsilon_{\rm GB} = 1$, and from Eq. 6 for $\epsilon_{\rm Junc} = \epsilon_{\rm GB} \leq -1$.

boundaries and to occupy the grain boundary regions due to the reduced $T_{\rm c}$ [23]. Preliminary calculations showed that results were not strongly dependent on the coating width. Fig. 2 shows the evolution of the average electric field in the x-direction E_x and $J_{\rm app}$ with time. In order to obtain the critical current density at each applied magnetic field, the system was first initialized in the Meissner state throughout and the applied magnetic field was rapidly ramped at a rate of $5 \times 10^{-2} B_{c2} \tau^{-1}$ to the set value. Next, the current was increased at $5 \times 10^{-6} J_{\rm D} \tau^{-1}$. At each timestep the average electric field in the x-direction was calculated. If it exceeded the electric field criterion of $10^{-5} E_{\rm D}$, the current is held constant for up to $2 \times 10^4 \tau$. If the electric field persisted above $10^{-5} E_{\rm D}$, $J_{\rm app}$ was associated with persistent vortex motion and taken to be the critical current density of the system. If $E_x < 10^{-5} E_{\rm D}$ the high E-field is associated with a transient flux jump and the current was ramped up further until $J_{\rm c}$ was reached. Such a transient event can be seen in the local plateau in the dashed $J(t)$ line in Fig. 2 at $t \approx 4000\tau$. The higher the applied magnetic field of the system, the lower the applied current at which the first vortex jump occurs and the longer the duration of a single transient event. This increased duration can be attributed to the reduced Lorentz force acting on a single vortex at low currents in high fields, which results in slower motion and equilibration of the vortices.

The standard mesh step size (i.e., $h_x = h_y = 0.5\xi_{\rm s}$) used in these simulations results in rasterization of the Voronoi tessellation and 'staircasing' of the grain boundary regions. However Fig. 3 demonstrates that the critical current behavior as a function of field is not strongly affected by mesh size. We chose a standard mesh step size of $0.5\xi_{\rm s}$ since it gave the optimal trade-off between accuracy and computation time.

The critical current density as a function of field $J_{\rm c}(B)$ for the polycrystal system of Fig. 1 is presented in Fig. 4, and can be compared to equivalent curves obtained for a single Josephson junction system in Fig. 5. When $\epsilon_{\rm GB} = 1.0$, there are no grain boundaries or barriers in the superconductor so the $J_{\rm c}$ values are identical in these two figures. $J_{\rm c}$ can be attributed to surface pinning from the two superconducting surfaces in contact with the coating region, with a surface area per unit volume of surface pins $S = 2/w_{\rm s}$, and a critical current density dependence given by [24]

$$J_{\rm c}^{\epsilon=1.0} = \frac{\xi_{\rm s}}{2w_{\rm s}} b^{-0.5} (1-b)^2 J_{\rm D}, \tag{5}$$

where $b = B_{\rm app}/B_{c2}$. $J_{\rm c}$ data for $\epsilon_{\rm GB}$ and $\epsilon_{\rm Junc} \leq -1.0$ in Fig. 4 and 5 display Josephson junction behavior. We have used the semi-empirical low field critical current dependence for Josephson junction systems, with the factor $(1-b)^2$ added

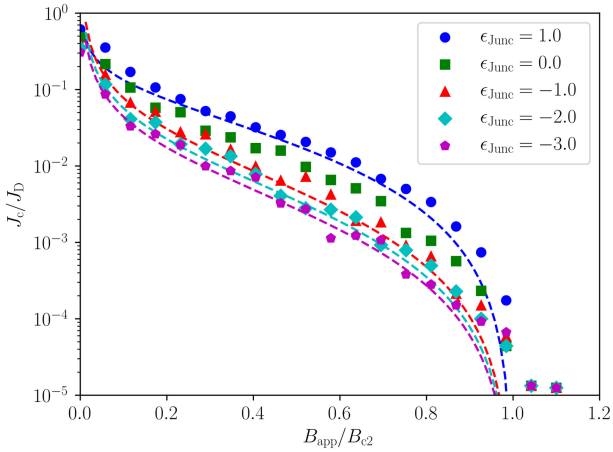

Fig. 5. Critical current density J_c of a simple junction system as a function of applied magnetic field $B_{\rm app}$ for different T_c in the junction region. We have used $h_x = h_y = 0.5\xi, w_s = 25\xi, l = 60\xi, \eta = 5.79$ and $\kappa = 5$. $\epsilon_{\rm Junc} = 1.0$ corresponds to a homogeneous superconductive system, with no reduction of T_c in the grain boundary regions. Dashed lines represented predicted $J_c(B)$ from Eq. 5 for $\epsilon_{\rm Junc} = 1$, and from Eq. 6 for $\epsilon_{\rm Junc} \leq -1$.

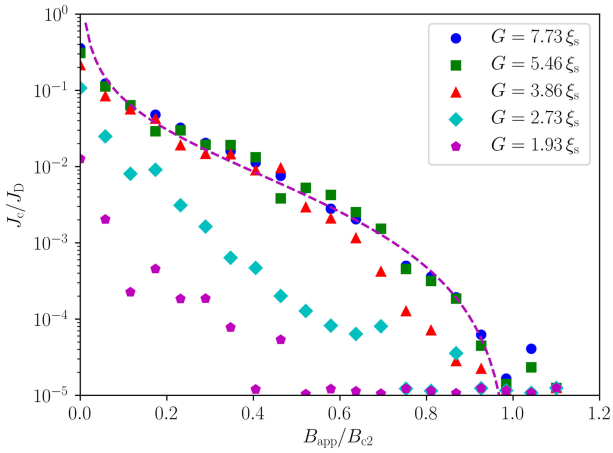

Fig. 6. Critical current density J_c as a function of applied magnetic field $B_{\rm app}$ for the Voronoi polycrystalline system shown in Fig. 1 for different grain diameters G. We have used $h_x = h_y = 0.5\xi$, $w_s = 25\xi$, $l = 60\xi$, $\eta = 5.79$ and $\kappa = 5$. In the large grain size regime, grain size does not have a significant effect on J_c For small grain sizes, J_c is reduced by the proximity effect. Dashed line represents predicted $J_c(B)$ from Eq. 6 with $\epsilon_{\rm Junc} = \epsilon_{\rm GB} = -1$.

to extend the functional form to high-fields [25]:

$$J_c = \frac{J_{DJ}\xi_s^2}{\sqrt{2}\, w_s\, (d\, + 2\xi_s)}\, b^{-1}(1-b)^2,$$

$$J_{DJ} = 2J_D\, u\left(u^2 - u\,\sqrt{u^2+2}+1\right) e^{-du/\xi_s}, \qquad (6)$$

where $u = \sqrt{-\epsilon_{\rm Junc}}$. In Eqns. 6 and 7, we find $J_c \propto 1/w_S$ which indicates J_c is determined predominantly by surface pinning. We also note that J_c in all polycrystalline simulations is less than the corresponding single-junction case at all fields. In Fig. 6, we present data that show J_c is independent of grain size at large grain sizes, suggesting that bulk pinning is negligible in these simulations, as the contribution from bulk pinning is expected to increase as grain size decreases. Only when the average grain diameter G is sufficiently small that the average superparticle density in the system is limited by the proximity effect of the grain boundary regions does the critical current density become sensitive to changes in the system grain size. Furthermore, the independence of J_c when G is large for a range of different meshes is consistent with the conclusions from this work not being sensitive to variations in the specific locations of the initial seed points used to generate any particular large grain Voronoi mesh (e.g., Fig. 1).

V. Discussion and Future Work

We expect the classic Voronoi tessellation used here to exhibit some of the key characteristics of grain boundaries in polycrystalline systems, including no large-scale periodicity in the direction of vortex flow and the effects from the additional pinning at the intersection of boundary regions. Hence we anticipate the broad features identified in the $J_c(B)$ characteristics presented here to be physically reasonable. However in future work, we will investigate other seeding possibilities since starting from a uniformly distributed set of seed points is known to underestimate the variation in grain size in real polycrystalline systems; in particular, large grains [8]. To describe the grain size distribution of a superconductor such as Nb_3Sn more realistically, we will consider selecting the set of seed points used to generate the tessellation from a weighted distribution [8]. Here we have treated all grain boundaries as regions with locally reduced T_c, and have not attempted to include local changes in the grain boundary resistivity through a spatially dependent effective mass term. We will investigate increasing the resistivity in grain boundary regions. This will increase intragranular currents running along the boundaries and the upper critical field of the overall system. Naturally, we also intend to consider three-dimensional Voronoi polycrystalline systems.

VI. Conclusion

We have used Voronoi tessellations to simulate vortex flow along grain boundaries in two-dimensional polycrystalline superconductors and found J_c values that are similar to those found in technological superconductors [1]. In the simulations presented here, surface pinning is generally much stronger than bulk pinning for large grain sizes. Only when the grain sizes are small ($\sim \xi_s$) is J_c limited by grain size because it is reduced by the proximity effect. The primary effects of the grain boundaries in our simulations is to provide preferred channels for flux flow across the superconductor and to reduce the surface barrier and hence J_c at all fields. Future work will include simulations of real 3D polycrystalline systems since the approach adopted here is in principle simply scalable.

Acknowledgment

The authors would like to thank A. Smith, M. Raine and P. Branch for useful discussions. This work made use of the facilities of the Hamilton HPC Service of Durham University. Data are available at doi:10.15128/r1pr76f341x and associated materials are on the Durham Research Online website: http://dro.dur.ac.uk/.

REFERENCES

[1] G. Wang, M. J. Raine, and D. P. Hampshire, "How resistive must grain-boundaries be to limit J_C in polycrystalline superconductors?," *Supercond. Sci. Technol.*, vol. 30, no. 10, 2017, Art. no. 104001.

[2] G. R. Berdiyorov *et al.*, "Dynamic and static phases of vortices under an applied drive in a superconducting stripe with an array of weak links," *The Eur. Phys. J. B*, vol. 85, no. 4, p. 130, Apr. 24, 2012.

[3] G. J. Carty and D. P. Hampshire, "Visualising the mechanism that determines the critical current density in polycrystalline superconductors using time-dependent Ginzburg-Landau theory," *Phys. Rev. B*, vol. 77, 2008, Art. no. 172501.

[4] I. A. Sadovskyy, A. E. Koshelev, A. Glatz, V. Ortalan, M. W. Rupich, and M. Leroux, "Simulation of the vortex dynamics in a real pinning landscape of $YBa_2Cu_3O_{7-\delta}$ coated conductors coated conductors," *Phys. Rev. Appl.*, vol. 5, no. 1, Jan. 27, 2016, Art. no. 014011.

[5] I. A. Sadovskyy, A. E. Koshelev, C. L. Phillips, D. A. Karpeyev, and A. Glatz, "Stable large-scale solver for Ginzburg–Landau equations for superconductors," *J. Comput. Phys.*, vol. 294, pp. 639–654, Aug. 1, 2015.

[6] G. Kimmel, I. A. Sadovskyy, and A. Glatz, "In silico optimization of critical currents in superconductors," *Phys. Rev. E*, vol. 96, no. 1, Jul. 27, 2017, Art. no. 013318.

[7] A. E. Koshelev, I. A. Sadovskyy, C. L. Phillips, and A. Glatz, "Optimization of vortex pinning by nanoparticles using simulations of the time-dependent Ginzburg-Landau model," *Phys. Rev. B*, vol. 93, no. 6, Feb. 29, 2016, Art. no. 060508.

[8] T. Luther and C. Könke, "Polycrystal models for the analysis of intergranular crack growth in metallic materials," *Eng. Fracture Mech.*, vol. 76, no. 15, pp. 2332–2343, Oct. 2009.

[9] R. Quey, P. R. Dawson, and F. Barbe, "Large-scale 3D random polycrystals for the finite element method: Generation, meshing and remeshing," *Comput. Methods Appl. Mech. Eng.*, vol. 200, no. 17, pp. 1729–1745, Apr. 2011.

[10] G. Dezanneau, A. Morata, A. Tarancón, M. Salleras, F. Peiró, and J. R. Morante, "Grain-boundary resistivity versus grain size distribution in three-dimensional polycrystals," *Appl. Phys. Lett.*, vol. 88, no. 14, 2006, Art. no. 141920.

[11] L. P. Gor'kov and G. M. Eliashberg, "Generalization of the Ginzburg-Landau equations for non-stationary problems in the case of alloys with paramagnetic impurities," *Sov. Phys. JETP*, vol. 27, no. 2, pp. 328–334, 1968.

[12] J. Fleckinger-Pelle and H. G. Kaper, "Gauges for the Ginzburg-Landau equations of superconductivity," in *Proc. Conf.: Int. Congr. Industrial Appl. Math.*, Hamburg, Germany, Jul. 3–7, 1995.

[13] N. B. Kopnin, B. I. Ivlev, and V. A. Kalatsky, "The flux-flow hall effect in type II superconductors. An explanation of the sign reversal," *J. Low Temp. Phys.*, vol. 90, no. 1, pp. 1–13, Jan. 1993.

[14] A. Schmid, "A Time dependent Ginzburg-Landau Equation and its Application to the problem of resistivity in the Mixed State," *Physik der Kondensierte Materie*, vol. 5, pp. 302–317, 1966.

[15] P. G. De Gennes, *Superconductivity of Metals and Alloys*. Boulder, CO, USA: Perseus Books Group, 1999.

[16] T. Winiecki and C. S. Adams, "A fast semi-implicit finite difference method for the TDGL equations," *J. Comput. Phys.*, vol. 179, pp. 127–139, 2002.

[17] W. D. Gropp *et al.*, "Numerical simulation of vortex dynamics in Type-II superconductors," *J. Comput. Phys.*, vol. 123, pp. 254–266, 1996.

[18] W. F. Ames, *Numerical Methods for Partial Differential Equations*. San Diego, CA, USA: Academic, 1992.

[19] W. H. Press, B. P. Flannery, S. A. Teukolsky, and W. T. Vetterling, *Numerical Recipes in Fortran: The Art of Scientific Computing*, 2nd ed. Cambridge, U.K.: Cambridge Univ. Press, 1992.

[20] O. Schenk and K. Gärtner, "Solving unsymmetric sparse systems of linear equations with PARDISO," *Future Gener. Comput. Syst.*, vol. 20, no. 3, pp. 475–487, Apr. 2004.

[21] J. Jordan, pyvoro Python wrapper for Voro++(2014). Accessed: Oct. 28, 2018. [Online]. Available: github.com/joe-jordan/pyvoro.

[22] C. H. Rycroft, "VORO++: A three-dimensional Voronoi cell library in C++," *Chaos: An Interdisciplinary J. Nonlinear Sci.*, vol. 19, no. 4, 2009, Art. no. 041111.

[23] P. Sunwong, J. S. Higgins, Y. Tsui, M. J. Raine, and D. P. Hampshire, "The critical current density of grain boundary channels in polycrystalline HTS and LTS superconductors in magnetic fields," *Supercond. Sci. Technol.*, vol. 26, 2013, Art. no. 095006.

[24] D. Dew-Hughes, "Flux pinning mechanisms in type II superconductors," *Philosophical Mag.*, vol. 30, no. 2, pp. 293–305, 1974.

[25] G. J. Carty and D. P. Hampshire, "The critical current density of an SNS junction in high magnetic fields," *Supercond. Sci. Technol.*, vol. 26, 2013, Art. no. 065007.